Solid State Ionics 48 (1991) 139–154
North-Holland

SOLID
STATE
IONICS

Electrode polarization at the $Au,O_2(g)$/yttria stabilized zirconia interface. Part I: Theoretical considerations of reaction model

B.A. van Hassel, B.A. Boukamp and A.J. Burggraaf

Laboratory for Inorganic Chemistry, Materials Science and Catalysis, Department of Chemical Technology, University of Twente, P.O. Box 217, 7500 AE Enschede, The Netherlands

Received 3 January 1991; accepted for publication 6 August 1991

Three different reaction models are discussed which describe the oxygen exchange reaction at the $Au,O_2(g)$/yttria stabilized zirconia interface. The first model assumes the charge transfer process to be rate determining. If the electron transfer to the adsorbed oxygen species occurs in a stepwise fashion low frequency inductive effects can be simulated in the frequency dispersion of the electrode impedance. If the charge transfer process is in competition with mass transport of oxygen along the $Au,O_2(g)$/ stabilized zirconia interface the second model can predict "apparent" Tafel behaviour of the current-overpotential curve. The real charge transfer coefficients change from $\alpha_c = \alpha_a = 1$ to apparent values of $\alpha_c = 0.5$ and $\alpha_a = 1.5$. Due to a gradient in the fraction of coverage of the molecular adsorbed oxygen species along the $Au,O_2(g)$/stabilized zirconia interface, the oxygen partial pressure dependence of the equilibrium exchange current density changes from $I_0 \propto P_{O_2}^{1/4}$ to $I_0 \propto P_{O_2}^{5/8}$. Depending on the basic charge transfer mechanism inductive effects at the electrode remain possible. The electrode impedance derived from this model under equilibrium conditions thus far revealed only capacitive effects. This makes this reaction model difficult to distinguish from the electrode impedance of a pure charge transfer process with an adsorbed intermediate. In case the mass transport process is rate determining limiting currents are predicted at moderate values of the applied overpotential. The electrode impedance then consists of a finite-length Warburg diffusion element and inductive effects cannot be predicted.

1. Introduction

Yttria stabilized zirconia is used as an oxygen ion conducting solid electrolyte in applications like oxygen sensors, oxygen pumps and fuel cells [1]. In all those devices an exchange occurs between oxygen from the gas phase and the oxygen ions in the solid electrolyte. The rate of this exchange reaction determines partly the response time of YSZ based oxygen sensors, it determines the rate at which oxygen can be transported through an oxygen pump and when the ohmic losses in a fuel cell are low enough it determines the efficiency of a fuel cell.

The exchange of oxygen between the gas and the electrolyte can be described with the following overall reaction:

$$O_2 + 2\,V_O^{\bullet\bullet} + 4\,e^- \rightleftarrows 2\,O_O^x \qquad (1)$$

where, in Kröger-Vink notation, $V_O^{\bullet\bullet}$ is an oxygen vacancy and O_O^x is a normal O^{2-} ion in the YSZ lattice. This overall reaction can be decomposed into at least three successive steps: a) adsorption, b) diffusion, c) charge transfer. Before any charge transfer can take place oxygen is adsorbed either on the noble metal surface or on the surface of the solid electrolyte. The adsorbed oxygen diffuses towards the electrochemical reaction sites at the three phase boundary between the solid electrolyte, the noble metal electrode and the gas phase or towards the reaction sites at the interface between the noble metal electrode and the solid electrolyte. At those sites, the charge transfer towards the adsorbed oxygen species is presumed to take place. When the solid electrolyte surface is mixed conducting, i.e. exhibiting both ionic and electronic conductivity, the oxide surface itself can be active in the charge transfer process and the role of the metal may be that of a current collector.

In literature three types of reaction models can be distinguished which describe the oxygen exchange reaction. The first model assumes that the charge transfer at the noble metal electrode is rate determining [2-4]. The second model assumes a competition between charge transfer and mass transport of adsorbed

oxygen species along the interface between the noble metal electrode and the solid electrolyte [5-9]. The third model assumes that the rate of charge transfer across the electrode/solid electrolyte interface is infinitely fast and that either adsorption/desorption of oxygen at the three phase boundary or diffusion of oxygen species towards the three phase boundary is rate determining [3,10-12].

In this paper our interest is focused on the consequences of these models for the expressions of the steady state current voltage characteristic and the electrode impedance. This evaluation of the reaction models is made in order to obtain a theoretical background for the discussion of experimental results obtained on the electrode polarisation at the Au,O_2(g)/yttria stabilized zirconia interface [13]. Apparent Tafel behaviour has been observed in those measurements in combination with inductive loops in the impedance diagram during cathodic and anodic polarisation. Especially the origin of inductive loops in the impedance diagram is discussed in some detail. Au electrodes were chosen in this study as gold is considered to be inactive in reaction (1). Thus the influence of the metal can be minimized.

2. Reaction Models

2.1. *Charge transfer model*

Many charge transfer mechanisms have been proposed in literature [2-4] for the oxygen exchange reaction. Different adsorbed oxygen species were assumed to be present like: $O_{2,ad}$, $O_{2,ad}$, O_{ad}, O_{ad}, etc. Some of the adsorbed oxygen species were identified with spectroscopic techniques (ESR [14-17], IR [18]). In studies of the oxygen exchange reaction the main emphasis has been on the different Tafel slopes and oxygen partial pressure dependencies of the equilibrium exchange current density (I_o) predicted by the selected reaction model. Little attention has been paid to the effect of the adsorbed intermediates in the selected reaction model on the electrode impedance.

The following hypothetical mechanism for the oxygen transfer at the Au,O_2(g)/stabilized zirconia interface is chosen in order to illustrate the calculation method of the steady state current-overpotential curve and the electrode impedance:

$$O_{2,gas} + 2\,ad \underset{k_{des}}{\overset{k_{ad}}{\rightleftarrows}} 2\,O_{ad} \qquad (2a)$$

$$2 \times \left(O_{ad} + e^{-} \underset{k_{o2}}{\overset{k_{r2}}{\rightleftarrows}} O_{ad}^{-} \right) \qquad (2b)$$

$$2 \times \left(O_{ad} + e^{-} + V_O^{\bullet\bullet} \underset{k_{o3}}{\overset{k_{r3}}{\rightleftarrows}} O_O^{x} + ad \right) \qquad (2c)$$

Oxygen adsorbs dissociatively at an adsorption site (=ad). In each of the following steps one electron is transferred to the adsorbed oxygen atom, which is finally incorporated by means of an oxygen vacancy in the stabilized zirconia lattice. The surface diffusion of the adsorbed oxygen species is assumed to be infinitely fast. This is one of the reaction models that explains inductive effects at the electrode. Those inductive effects are experimentally observed at low frequencies in the impedance diagram during both anodic and cathodic polarisation.

2.1.1. *Steady-state behaviour*

The reaction scheme given above can be translated into a series of mathematical expressions using some hypotheses. The main hypotheses concern the potential dependence of the reaction rate constants and an adsorption isotherm law. This calculation method has often been applied in aqueous electrochemistry [19-22].

It is assumed that the potential (E) dependence of the reaction rate constants is given by the so called Tafel-law [23]:

$$k_{ri} = k_{ri}^{o} \exp(-\beta_i n_i F E/RT) \qquad (3)$$

$$k_{oi} = k_{oi}^{o} \exp((1-\beta_i) n_i F E/RT) \qquad (4)$$

where β_i is the symmetry coefficient which is in the range: $0<\beta_i<1$ and n_i is the number of electrons transferred in the reaction step i. All reaction steps are assumed to proceed reversibly. What can happen in one direction can also happen in the opposite direction.

The intermediate oxygen species O_{ad} and O_{ad}^{-} occupy the fractions θ_1 and θ_2 of the reaction sites, respectively. The adsorption-desorption is assumed to follow a Langmuir-type isotherm-law. Although this adsorption model may be too simple, it makes the derivation of the impedance and polarisation relation easier to handle and it allows direct comparison with other models that are also based on the Langmuir isotherm-law [7,8]. No overlapping of the coverages is considered, hence $\theta_1+\theta_2 \leq 1$. Also no interaction between the adsorbed oxygen species is taken into account. The time dependence of the fraction of coverage of the adsorbed intermediates is given by the following mass balance equations:

$$\frac{d\Gamma\theta_1}{dt} = 2k_{ad}P_{O_2}(\Gamma(1-\theta_1-\theta_2))^2 - 2k_{des}(\Gamma\theta_1)^2 + -k_{r2}\Gamma\theta_1 + k_{o2}\Gamma\theta_2 \quad (5)$$

and:

$$\frac{d\Gamma\theta_2}{dt} = k_{r2}\Gamma\theta_1 - k_{o2}\Gamma\theta_2 + -k_{r3}\Gamma\theta_2 V_O^{\bullet\bullet} + k_{o3}O_O^x\Gamma(1-\theta_1-\theta_2) \quad (6)$$

where Γ is the maximum number of adsorption sites per unit area and is assumed to be independent of the electrode voltage and time. At steady state we have:

$$\frac{d\Gamma\theta_1}{dt}=0 \ , \ \text{and:} \quad \frac{d\Gamma\theta_2}{dt}=0 \quad (7)$$

From the eqs (5-7) the fraction of coverage of the adsorbed intermediates at steady state can be calculated when values are chosen for the reaction rate constants and symmetry coefficients. A suitable set of parameters is given in table 1. As eq. (5) is quadratic, two solutions are obtained for the fraction of coverage, θ_i. Only one of the solutions is physically possible ($\theta_i > 0$). The potential dependence of the fraction of coverage of the intermediate species O_{ad} and O^-_{ad}, based on the parameters of table 1, is shown in fig. 1. Whereas the fraction of coverage of the O_{ad} species is reasonably constant, the fraction of coverage of O^-_{ad} is strongly potential dependent. This potential dependence is very important for the electrode impedance, as is discussed in section 2.1.2.1.

Table 1 Reaction model parameters

parameter	value	dimension
k_{ad}	2.6×10^{13}	$mol^{-1}atm^{-1}m^2s^1$
k_{des}	1×10^{16}	$mol^{-1}m^2s^{-1}$
k_{r2}^o	1	s^{-1}
k_{o2}^o	6	s^{-1}
β_2	0.58	
k_{r3}^o	6×10^{-3}	$m^3mol^{-1}s^{-1}$
k_{o3}^o	1.714×10^{-6}	$m^3mol^{-1}s^{-1}$
β_3	0.10	
O_O^x	9.46×10^4	mol m^{-3}
$V_O^{\bullet\bullet}$	3.18×10^3	mol m^{-3}
Γ	8.17×10^{-6}	mol m^{-2}
C_{dl}	0.001	F m^{-2}
PO_2	1	atm
Temp.	763.4	°C
A	0.659×10^{-4}	m^2

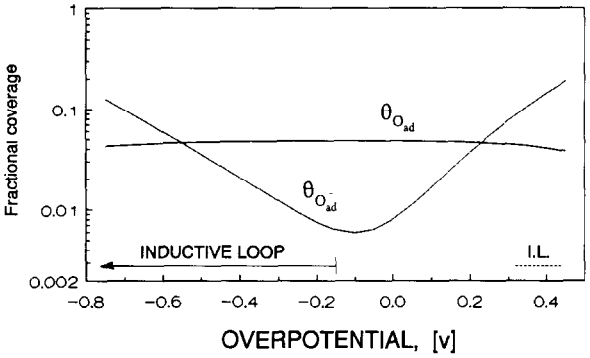

Fig.1 Fraction of coverage of the adsorbed oxygen species O_{ad} and O^-_{ad} as function of the overpotential for the reaction mechanism given by the eqs (2a-c). Parameters of table 1 are used in the simulation.

The faradaic current density is expressed as:

$$I_F = FA(k_{o2}\Gamma\theta_2 - k_{r2}\Gamma\theta_1) + +FA(k_{o3}O_O^x\Gamma(1-\theta_1-\theta_2) - k_{r3}V_O^{\bullet\bullet}\Gamma\theta_2) \quad (8)$$

where A is the electrode surface area. Thus the steady state polarization curve can be calculated by substituting the steady state values of the fraction of coverage of the adsorbed intermediate species and using suitable values for k_{ri}^o, k_{oi}^o and β_i. The potential dependence of the reaction rate constants is given by the eqs (3) and (4).

Under equilibrium conditions the net faradaic current (eq. 8) is zero. The corresponding equilibrium potential is given by the following expression:

$$E_{eq.} = \frac{RT}{2F}\ln\left[\frac{k_{r3}^o}{k_{o3}^o}\frac{k_{r2}^o}{k_{o2}^o}\frac{V_O^{\bullet\bullet}}{O_O^x}\sqrt{\frac{k_{ad}}{k_{des}}}\right] + \frac{RT}{4F}\ln\left(PO_2\right) \quad (9)$$

which is simply an equation of the Nernst form [22]. In this study the equilibrium potential which develops at a temperature of 763 °C and an oxygen partial pressure of PO_2=1 atm is arbitrarily set equal to zero. *In this way the electrode potential is defined relative to the equilibrium potential at 763°C and PO_2=1 atm.*

When local equilibrium is assumed for all steps except the rate determining step an expression for the current-voltage characteristic can be obtained using the models of Bockris and Reddy [23]. This results in Butler-Volmer relations with different values of the real charge transfer coefficients (α_a, α_c) and different PO_2 dependencies of the equilibrium exchange current density (I_o), depending on which step is rate determining:

$$I_F = I_o A(\exp(\alpha_a F\eta/RT) - \exp(-\alpha_c F\eta/RT)) \qquad (10)$$

where η (= E - E_{eq}) is the electrode overpotential. The general formulae relating the reaction model parameters to the real charge transfer coefficients are discussed in Appendix A.1. The equilibrium exchange current density, I_o, depends on the oxygen partial pressure according to:

$$I_o \propto \left(P_{O_2}\right)^m \qquad (11)$$

Values of the real charge transfer coefficients and PO_2 dependence of the equilibrium exchange current density for the reaction mechanism (2a-c) are shown in table 2, assuming the fraction of coverage of the adsorbed intermediates to be small ($\theta_i << 1$).

A simulation of the current-overpotential characteristic of eq. (8) is shown in fig. 2a, together with an experimentally observed current-overpotential characteristic (Au, O_2(gas)/YSZ, PO_2=1atm, 763 °C [13]). Figure 2b shows the corresponding Tafel-plots. The simulated current-overpotential characteristic was obtained by choosing six rate constants in the reaction mechanism of eq. (2a-c), for which the values are given in table 1. The potential dependence of the faradaic current density is insensitive to the adsorption and desorption rate constants (k_{ad}, k_{des}) as this reaction step (2a) has been chosen not to be rate determining. By choosing a certain value for the adsorption and desorption rate constants, the fraction of coverage of O_{ad} and the current density at the electrode could be controlled. The reaction rate constants of step (2b) and (2c) were chosen so that reaction step (2b) was rate determining. Although the cathodic part of the measured polarisation curve is simulated fairly well, serious deviations occur at anodic overpotentials. This simulation could be improved by taking other values of the rate constants, but this resulted in a poor simulation of the electrode impedance (discussed in section 2.1.2.).

An alternative way for improving the computer simulation of the anodic part of the current-overpotential characteristic was to add an additional step to the reaction mechanism (given in the eq. 2a-c):

Table 2 Influence of the choice of the rate determining step in eq. (2a-c) on the cathodic and anodic charge transfer coefficients in the Butler-Volmer relation of eq.(10). The PO_2 dependence of the exchange current density (m) is given by eq. (11).

rds	α_c	α_a	m
2a	0	4	1
2b	0.5	1.5	3/8
2c	1.5	0.5	1/8

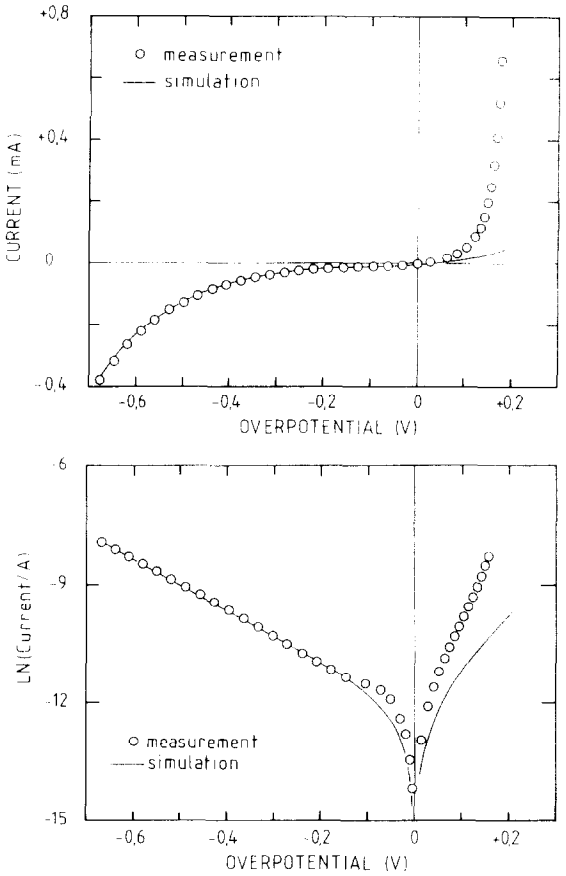

Fig.2 a) Experimentally determined current-overpotential curve (763 °C, PO_2=1atm) in comparison with simulated curve using the reaction model of eqs (2a-c). For the simulation the values of table 1 are used. b) Corresponding Tafel plots.

$$O_2 + V_O^{\bullet\bullet} + 3e^- \underset{k_{o3}}{\overset{k_{r3}}{\rightleftarrows}} O_O^x + O_{ad}^- \qquad (12)$$

This reaction step is meant as a special adsorption/desorption reaction and improved the simulation of both the experimentally observed current-overpotential curve and electrode impedance considerably. Reaction (12), however, should not be taken as an elementary charge transfer reaction as the simultaneous transfer of three electrons is physically unlikely. Hence reaction (12) indicates a different mechanism for the oxygen evolution reaction parallel to the the reactions (2a-c), and will be composed of several other reaction steps. Although an improved fit to the current-overpotential curve was obtained the PO_2 dependence of the equilibrium exchange current density (m=0.29) was smaller than experimentally observed (m=0.60±0.02).

In general it can be concluded that if a charge transfer process is rate determining, then Butler-Volmer type current voltage characteristics are obtained. The current density at the electrode depends exponentially on the applied overpotential.

2.1.2. *Electrochemical impedance*

2.1.2.1. *Adsorbed intermediates*

When a sinusoidal perturbation of small amplitude, $\Delta E.\exp(j\omega t)$, is added to the applied potential difference E, the corresponding current, $\Delta I.\exp(j\omega t)$, is modulated in sinusoidally around its steady state value I_F, where $j^2=-1$. Expanding eq. (8) in to a Taylor series, limited to first order terms, the following expression is obtained for the amplitude of the current modulation [19]:

$$\Delta I_F = \left(\frac{dI_F}{dE}\right)_{\theta_1,\theta_2} \Delta E + \left(\frac{dI_F}{d\Gamma\theta_1}\right)_{E,\theta_2} \Delta\Gamma\theta_1 + \left(\frac{dI_F}{d\Gamma\theta_2}\right)_{E,\theta_1} \Delta\Gamma\theta_2 \qquad (13)$$

from which the Faradaic impedance, Z_F, can be obtained:

$$Z_F = \left(\frac{\Delta E}{\Delta I_F}\right) = R_{ct} + Z_{\theta_1} + Z_{\theta_2} \qquad (14)$$

where:

$$R_{ct} = \left(\frac{dI_F}{dE}\right)^{-1}_{\theta_1,\theta_2} \qquad (15)$$

$$Z_{\theta_1} = -\left(\frac{\left(\frac{dI_F}{d\Gamma\theta_1}\right)_{E,\theta_2}}{\left(\frac{dI_F}{dE}\right)_{\theta_1,\theta_2}}\right)\frac{\Delta\Gamma\theta_1}{\Delta I_F} \qquad (16)$$

$$Z_{\theta_2} = -\left(\frac{\left(\frac{dI_F}{d\Gamma\theta_2}\right)_{E,\theta_1}}{\left(\frac{dI_F}{dE}\right)_{\theta_1,\theta_2}}\right)\frac{\Delta\Gamma\theta_2}{\Delta I_F} \qquad (17)$$

In the eqs (13), (16) and (17) $\Delta\Gamma\theta_i$ is the amplitude of the modulation of the fraction of coverage of the adsorbed species i around its steady state value, $\langle\Gamma\theta_i\rangle$ such that:

$$\Gamma\theta_i(t) = \langle\Gamma\theta_i\rangle + \Delta\Gamma\theta_i e^{j\omega t} \qquad (18)$$

Expressions for $\Delta\Gamma\theta_i/\Delta I_F$ in the eqs (16) and (17) are obtained by linearizing the eqs (5) and (6), which describe the mass balance at the electrode:

$$j\omega\Delta\Gamma\theta_1 = \frac{d}{dE}\left(\frac{d\Gamma\theta_1}{dt}\right)_{\theta_1,\theta_2}\Delta E + \frac{d}{d\Gamma\theta_1}\left(\frac{d\Gamma\theta_1}{dt}\right)_{E,\theta_2}\Delta\Gamma\theta_1 + \frac{d}{d\Gamma\theta_2}\left(\frac{d\Gamma\theta_1}{dt}\right)_{E,\theta_1}\Delta\Gamma\theta_2 \qquad (19)$$

and:

$$j\omega\Delta\Gamma\theta_2 = \frac{d}{dE}\left(\frac{d\Gamma\theta_2}{dt}\right)_{\theta_1,\theta_2}\Delta E + \frac{d}{d\Gamma\theta_1}\left(\frac{d\Gamma\theta_2}{dt}\right)_{E,\theta_2}\Delta\Gamma\theta_1 + \frac{d}{d\Gamma\theta_2}\left(\frac{d\Gamma\theta_2}{dt}\right)_{E,\theta_1}\Delta\Gamma\theta_2 \qquad (20)$$

Substitution of the expressions for $\Delta\Gamma\theta_1$ and $\Delta\Gamma\theta_2$ from the eqs (19) and (20) into eq. (13) results in analytic

expressions for the faradaic impedance of the electrode (Appendix A.2).

The charge transfer resistance in eq. (14) describes the faradaic impedance assuming that the fraction of coverage of the adsorbed oxygen species is constant. $Z_{\theta 1}$ and $Z_{\theta 2}$ are additional impedances due to changes of the fraction of coverage of the adsorbed oxygen species when the electrode potential is modulated.

The total impedance of the electrode is calculated assuming that a double layer capacitance, C_{dl}, is associated in parallel with the Faradaic impedance and that this double layer capacitance is independent of the electrode potential and the fraction of coverage of the adsorbed species:

$$Z = \left(\frac{Z_F}{1 + j\omega C_{dl} Z_F} \right) \qquad (21)$$

The final result is presented in the equivalent circuit of fig. 3. In this equivalent circuit all elements, except the double layer capacitance, C_{dl}, are potential dependent and can be calculated form the equations given in Appendix A.2. The Faradaic impedance of the electrode consists of a charge transfer resistance, R_{ct}, and a parallel combination of resistances R1, R2, a capacitance C_{ad} and an inductance L_{ad}. That part of the equivalent circuit standing in series with the charge transfer resistance represents the electrode impedance due to both $Z_{\theta 1}$ and $Z_{\theta 2}$. So this part reflects the additional impedance due to a change of the fraction of coverage of the adsorbed intermediates θ_1 and θ_2 when the electrode potential is modulated.

It is very difficult to find a combination of rate constants that result in an inductive loop at cathodic overpotentials and capacitive loops at anodic overpotentials. Depending on the values of the rate constants either the charge transfer resistance in parallel to the double layer capacitance or an additional capacitive loop was simulated. Computer simulations of the electrode impedance at various overpotentials, using the values for the kinetic constants of table 1 are shown in fig. 4. At low frequencies an inductive loop can be simulated when a cathodic overpotential is applied of $\eta < -0.1$ V, as shown in the figs 4a and b. At a cathodic polarisation of $\eta = -0.1$ V only the semicircle related to the double layer capacitance C_{dl} in parallel to the charge transfer resistance is simulated, as shown in fig. 4c. When the electrode is in equilibrium and during anodic polarisation a capacitive loop is simulated at low frequencies in the impedance diagram, as shown in figs 4d and 4e. A further increase of the anodic overpotential results again in an inductive loop, as shown in fig. 4f.

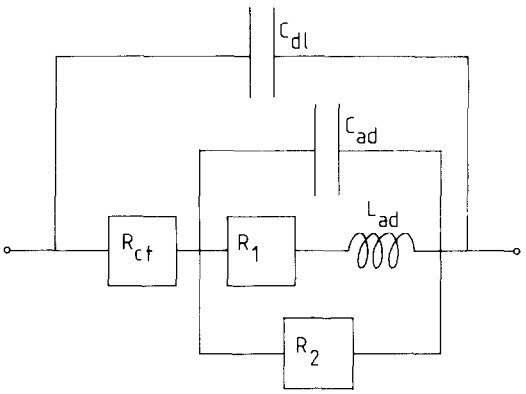

Fig.3 Equivalent circuit corresponding to the electrode impedance for the reaction mechanism of eqs (2a-c).

The occurrence of an inductive loop in the impedance diagram is closely related to the potential dependence of the adsorbed intermediates in the reaction mechanism. The parameters of table 1 result in a potential dependence of θ_1 and θ_2 which is shown in fig. 1. Whenever an increase is observed of θ_2 with a more negative cathodic overpotential, an inductive loop appears to be present, as shown in the impedance diagram of fig. 4a. In the minimum of the fraction of coverage θ_2 versus η curve, only the capacitive loop related to the parallel combination of the charge transfer resistance, R_{ct}, and double layer capacitance, C_{dl}, is present, resulting in the impedance diagram of fig. 4c. Both at equilibrium and during anodic polarisation an increase of θ_2 is observed with an increase in anodic polarisation. This resulted in the capacitive loop at low frequencies in the impedance diagram as shown in figs 4d and e. The inductive loop at high anodic overpotential appears when θ_1 (O_{ad}) starts to decrease, see fig. 1. A direct connection cannot be made due to the complexity of the impedance equation (Appendix A.2, eq. A17 - A22).

The reaction mechanism proposed is by no means the only mechanism that can explain inductive effects at an electrode. It has been chosen to illustrate the calculation method and proved to be useful in interpreting the experimental results. *In general it can be concluded that inductive effects may occur whenever a stepwise electron transfer takes place towards adsorbed intermediates. Whether the inductive effect appears in the impedance diagram will depend on the value of the rate constants and hence on the potential dependence of the fraction of coverage of the adsorbed intermediates.*

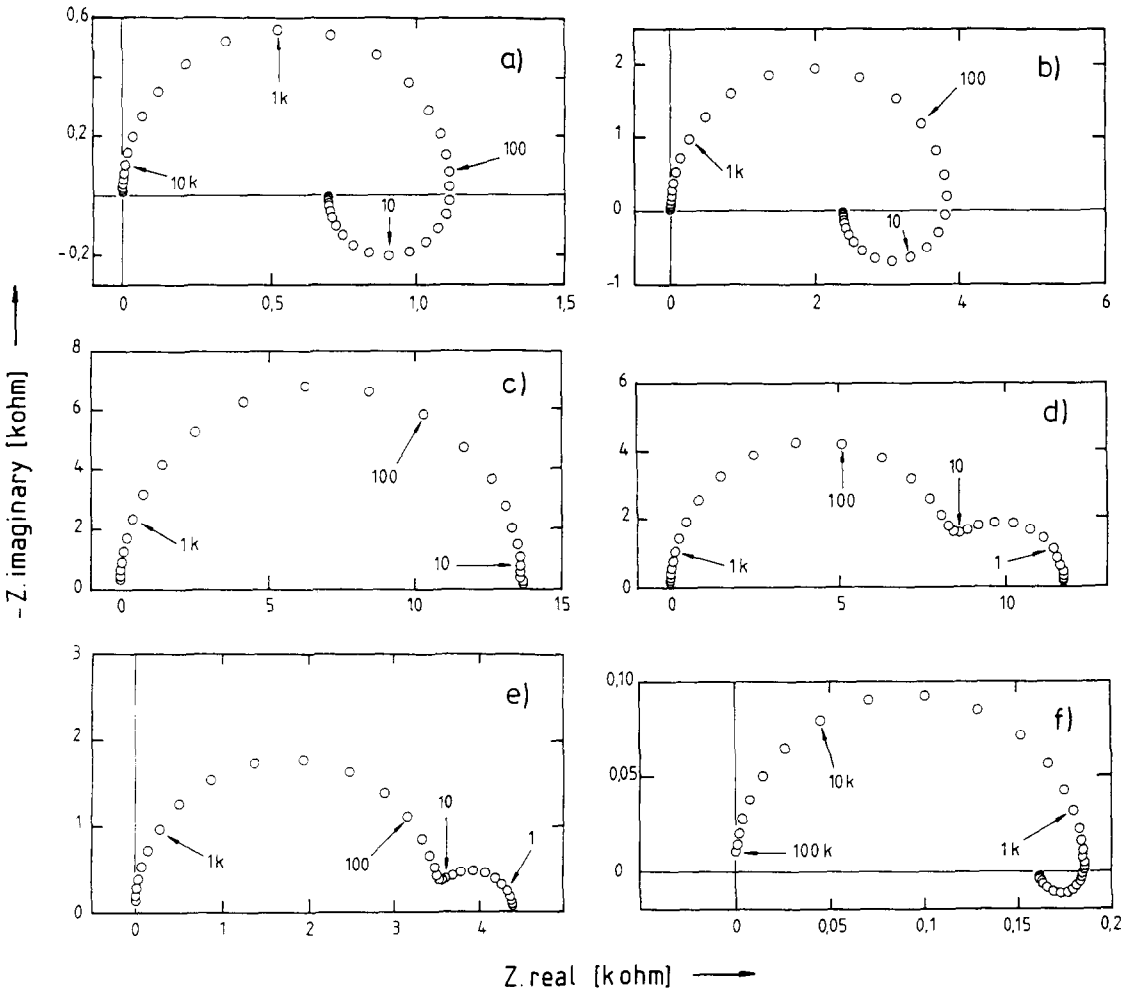

Fig.4 Electrode impedance as function of the overpotential according to the reaction mechanism of eq. (2) using parameters of table 1: a) η=-0.6 V, b) η=-0.4 V, c) η=-0.1 V, d) η=0 V, e) η=+0.1 V, f) η=+0.4 V. Frequencies indicated in Hz.

2.1.2.2. *Electrode surface area*

A more trivial reason for inductive effects at electrodes is the presence of a polarization dependence of the electrode surface area. Thus far the electrode surface area, A, has been assumed to be constant in time and independent of the polarization. The current at the electrode is given by eq. (8). If the electrode surface area is, however, potential dependent than the following expression for the electrode impedance is obtained:

$$Z_F = R_{ct} + Z_{\theta_1} + Z_{\theta_2} - \left[\frac{dI_F}{dA}\right]_{E,\theta_1,\theta_2} \frac{\Delta A}{\Delta E} \qquad (22)$$

The last term describes the fact that it will take a certain amount of time after a change in polarization in order to obtain a new value of the active electrode surface area. Depending on the sign of the ($\Delta A/\Delta E$) term, an inductive (($\Delta A/\Delta E$) > 0) or capacitive (($\Delta A/\Delta E$) < 0) effect may result in the impedance diagram.

The above interpretation has been strongly opposed by Epelboin [24] in the case of the electrocrystallisation of metals. Among other objections, the relatively large

change in electrode area, which was necessary to explain the experimental results, was never observed.

In the case of solid electrolytes little is known about either the absolute value of the electrode surface area or the exact position of the reaction sites. However, it has been argued by Schouler and Kleitz [25] and by Yanagida [26] that during anodic polarization holes are injected in the subsurface of yttria stabilized zirconia. The increase in the surface electronic carrier concentration is likely to result in a spreading of the electrode reaction zone. Due to the change in the electronic surface properties other reaction paths may become available, resulting in a further increase of the reaction rate and decrease of the electrode resistance.

2.2. *Charge transfer model in competition with mass transport*

2.2.1. *Steady-state behaviour*

The influence of mass transport on the charge transfer reaction at the interface between a noble metal electrode and an oxygen ion conducting solid electrolyte has been discussed by a number of authors [5-9]. In this section the expression for the current voltage characteristic is derived following the electrode geometry proposed by Wang and Nowick [5]. In their study the electrode is idealized as an array of metal strips as shown in fig. 5. The linear geometry is convenient for obtaining analytical results. More complex geometries were considered by Nguyen et al. [7] and Franceschetti and Ross [9], but similar results were obtained, at the expense of a greater mathematical complexity.

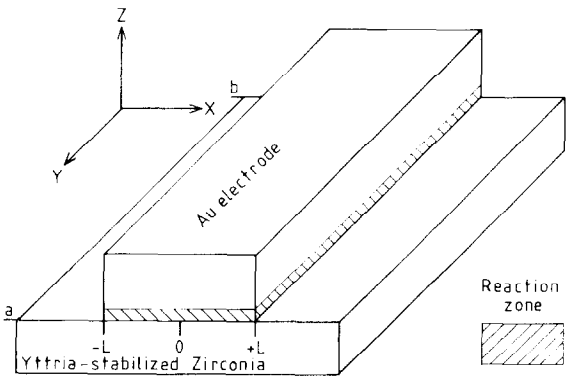

Fig.5 Idealized electrode geometry for a noble metal electrode on top of yttria stabilized zirconia with charge transfer and diffusion along the interface between the noble metal electrode and solid electrolyte surface.

The more exact treatment of Robertson and Michaels [8] is followed in order to obtain results, which are also valid at a high fraction of coverage of the adsorbed oxygen species (e.g at anodic overpotentials). Both the results for associative and dissociative adsorption of oxygen on either the solid electrolyte or noble metal electrode are discussed. The result for associative adsorption at an array of metal strips, which is also valid at a high fraction of coverage of the adsorbed oxygen species, has not yet been presented by others. In Part II [13,27], associative adsorption of oxygen will be shown to be the more appropriate reaction mechanism in the case of electrode polarisation at the Au,O_2(g)/yttria stabilized zirconia interface.

The mass transport is assumed to occur either by neutral oxygen molecules or oxygen atoms along the electrode/electrolyte interface. The diffusion of oxygen through the metal phase of the electrode can be neglected [28]. At equilibrium, the fraction of coverage (θ) of the adsorbed oxygen species, will be equal to their fraction of coverage outside this interface and no concentration gradient exists. Depending on whether the oxygen adsorbs associatively or dissociatively this results in the following values of the fraction of coverage, assuming a Langmuir adsorption isotherm:

$$\left(\frac{\theta}{1-\theta}\right)_{eq} = KP_{O_2} \quad \text{(associative)}$$
$$\left(\frac{\theta}{1-\theta}\right)_{eq} = \sqrt{KP_{O_2}} \quad \text{(dissociative)} \qquad (23)$$

When the electrode is polarized a concentration gradient builds up along this interface. This gradient depends on the interfacial diffusion rate as well as on the local charge transfer rate. The local charge transfer rate is assumed to follow a Butler-Volmer type of equation:

$$I_F = I_0 \left[\left(\frac{(1-\theta)}{(1-\theta_{eq})}\right) \exp(\alpha_a F\eta/RT) - \left(\frac{\theta}{\theta_{eq}}\right) \exp(-\alpha_c F\eta RT) \right] \qquad (24)$$

The real charge transfer coefficients are chosen to be: $\alpha_a=\alpha_c=1$. This implies also that the logarithm of I_0 depends on the logarithm of the oxygen partial pressure with a slope of $m=0.25$ if the fraction of coverage of the adsorbed oxygen species is small. The basic charge

transfer mechanism resulting in this Butler-Volmer equation can be obtained from the eqs (A.2-A.4) given in Appendix A.1 and is further discussed in Part II [13,27].

The fraction of coverage of the oxygen species between the Au electrode and the yttria stabilized zirconia surface is determined by the following mass balance equation:

$$\frac{d\Gamma\theta}{dt} = D\Gamma\frac{d^2\theta}{dx^2} + \frac{I_F}{n\,F} \tag{25}$$

where n is the total number of electrons transferred from the electrode to the diffusing oxygen species. In the case of molecular oxygen as diffusing species (associative adsorption), the total number of transferring electrons per reaction step is assumed to be equal to 4, whereas in the case of atomic oxygen (dissociative adsorption), the total number of transferring electrons per reaction step is assumed to be 2.

At steady state the fraction of coverage of the diffusing species is independent of time ($d\theta/dt=0$). Instead of using the coordinate x, the dimensionless coordinate $w=x/l$ is used. The edges of the metal strip are located at $w=\pm1$ and $w=0$ is the centre of the metal strip. Solutions for the fraction of coverage as a function of the distance w can be obtained from the eqs (24) and (25) when boundary conditions are specified at both $w=\pm1$ and $w=0$. The boundary condition at $w=0$ follows from the symmetry of the strip shaped electrode:

$$\left[\frac{d\theta}{dw}\right]_{w=0} = 0 \tag{26}$$

Various boundary conditions can be considered at $w=\pm1$. Here it is assumed that the fraction of coverage of oxygen species outside the electrode / electrolyte interface ($w\leq -1$ and $w\geq 1$) is in equilibrium with the gas phase and given by eq. (23). Solutions for other boundary conditions, which may result in limiting current behaviour, can be found in the literature [3,8].

For both associative and dissociative adsorption the solution of eq. (25) under steady state conditions is:

$$\theta(w) = \frac{-2\phi\sinh(\frac{F\eta}{RT})}{G^2}\,\frac{\cosh Gw}{\cosh G} + \frac{\phi\exp(\frac{F\eta}{RT})}{(1-\theta)_{eq}G^2} \tag{27}$$

where:

$$G^2 = \phi\left[\frac{\exp(\frac{F\,\eta}{RT})}{(1-\theta)_{eq}} + \frac{\exp(\frac{-F\,\eta}{RT})}{\theta_{eq}}\right] \tag{28}$$

$$\phi = \left[\frac{I_o L^2}{nFD\Gamma}\right] \tag{29}$$

For associative adsorption n=4 and for dissociative adsorption n=2 in eq. (29). Substitution of eq. (27) in eq. (24) results in:

$$I(w) = I_o\left[\frac{2\,\phi\,\sinh\frac{F\eta}{RT}}{G^2}\right]\frac{\cosh(G\,w)}{\cosh G} \tag{30}$$

which describes the local current density in the two phase region as a function of the dimensionless coordinate w. The total current per unit area of electrode is given by the integral over the plane of the electrode:

$$I_F = \frac{\int_a^b\int_{-1}^{+1} I(y,w)\,dw\,dy}{2(b-a)} \tag{31}$$

which can be shown to be:

$$I_F = 2\,I_o\sinh\left[\frac{F\eta}{RT}\right]\left[\frac{\tanh G}{G}\right] \tag{32}$$

Thus a competition between charge transfer and diffusion of adsorbed oxygen species along the electrode/solid electrolyte interface results in complicated current voltage curves. In the limiting case of small theta ($\theta << 1$) and large value of G eq. (32) reduces to:

$$I = I_o^*\left[\exp(+\frac{3}{2}\frac{F\eta}{RT}) - \exp(-\frac{1}{2}\frac{F\eta}{RT})\right] \tag{33}$$

This situation occurs when the charge transfer rate is large in comparison with the rate of diffusion in the interfacial region. Although a Butler-Volmer equation with real charge transfer coefficients of $\alpha_a=\alpha_c=1$ has been postulated for the charge transfer reaction, the competition with mass transport results in different 'apparent' transfer coefficients, i.e. $\alpha_a=1.5$, $\alpha_c=0.5$ as shown in fig. 6. The competition between mass transport and charge transfer results also in a change of the oxygen partial pressure dependence of the equilibrium exchange current density. When atomic oxygen diffuses, it changes from $I_o \propto PO_2^{1/4}$ to $I_o^* \propto PO_2^{3/8}$, whereas when molecular oxygen diffuses, it changes from $I_o \propto PO_2^{1/4}$ to $I_o^* \propto PO_2^{5/8}$.

Concentration profiles of the adsorbed oxygen

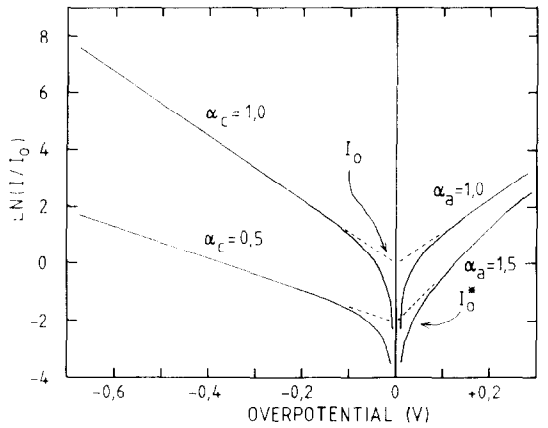

Fig.6 Simulated Tafel-plot of the current-over-potential curve for a small fraction of coverage of the adsorbed oxygen species and a large value of G, see eq. (32), with $\theta_{eq}=1x10^{-3}$, and $\phi=6.24x10^{-2}$.

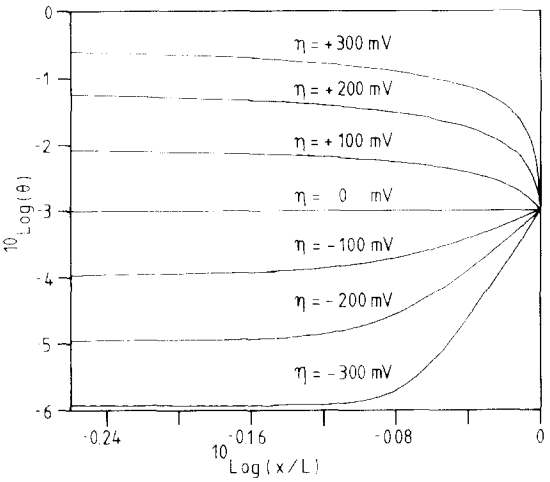

Fig.7 Fraction of coverage (θ) of molecular adsorbed oxygen species for cathodic and for anodic polarisation as function of the dimensionless coördinate w (eq. 27). Same parameters as in fig. 6 were used.

species at the electrode/solid electrolyte interface are shown in fig. 7. This figure shows that the highest fraction of coverage and hence the highest current density occurs at the edges of the metal strips during cathodic polarisation. At anodic overpotentials the fraction of coverage of the adsorbed oxygen species increases in the two phase region at the electrode/solid electrolyte interface due to mass transport limitations.

2.2.2. *Electrochemical impedance*

The consequences of this model for the Faradaic impedance of the electrode were explored in a theoretical analysis by Franceschetti and Ross [9]. When no overpotential is applied and the fraction of coverage of oxygen outside the two phase region equals the equilibrium coverage, it is possible to obtain the Faradaic impedance expression:
with:

$$Z_F = \frac{R_{ct}(1+j\Omega)}{(j\Omega+(\sqrt{K(1+j\Omega)}\coth(\sqrt{K(1+j\Omega)}))^{-1})} \qquad (34)$$

$K = k_{ob}\delta^2/D$
$\Omega = \omega/k_{ob}$

where:

ω = angular frequency of a sinusoidal signal ($\omega=2\pi f$)
k_{ob} = kinetic rate constant
L = width of contact strips
D = diffusion coefficient of oxygen species along the electrode/electrolyte interface
R_{ct} = the charge transfer resistance

A simulation of the electrode impedance, assuming that a double layer capacitance is in parallel with the faradaic impedance (eq. 34), is shown in fig. 8. The competition between charge transfer and diffusion results at the equilibrium potential, when the net faradaic current is zero, in a capacitive loop in the impedance diagram in addition to the capacitive loop related to the charge transfer resistance, R_{ct}, in parallel to the double layer capacitance, C_{dl}. Comparison of fig. 8 with fig. 4d indicates that it will be difficult to

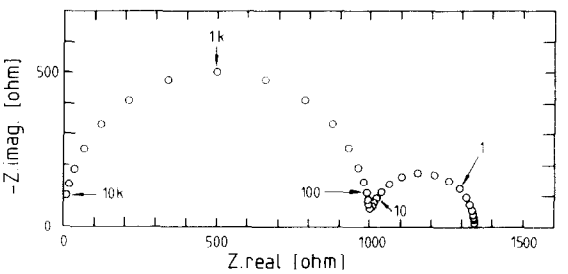

Fig.8 Electrode impedance for a reaction mechanism whith a competition between mass transport and charge transfer in the two phase region between the electrode and the solid electrolyte. The following parameters of eq. (34) were arbitrarily chosen to illustrate the shape of the impedance diagram: $C_{dl}=1x10^{-6}$F, $R_{ct}=1x10^{3}$ ohm, K=1.1, $k_{ob}=1$ sec^{-1}. Frequencies indicated in Hz.

distinguish the electrode impedance described in this section from the electrode impedance when a pure charge transfer mechanism with adsorbed intermediates is present.

To our knowledge no expressions for the electrode impedance under biased conditions have been published. When a stepwise electron transfer occurs to adsorbed intermediates in the basic charge transfer mechanism then inductive effects remain possible in the electrode impedance, but no exact treatment has been obtained.

2.3 *Mass transport model*

2.3.1 *Steady-state behaviour*

If the rate of electron exchange across the electrode/solid electrolyte interface is very fast, so that this interface is always in equilibrium with respect to the electron exchange, then the Nernst equation can be used to relate the overpotential to the deviation of the oxygen activity at the interface from the one in equilibrium:

$$\eta = \frac{RT}{4F}\ln\frac{P_{O_2,YSZ}}{P_{O_2,ref}} \qquad (35)$$

where:

$PO_{2,ref}$ = Oxygen partial pressure at unpolarized interface, in equilibrium with the gas phase.

$PO_{2,YSZ}$ = Oxygen partial pressure at polarized interface.

As pointed out by Bockris and Reddy [23], care should be taken not to use this equation for interpreting a situation far from equilibrium.

This approximation was followed by Mizusaki [11,12], studying the electrode reaction at the Pt,O_2(g)/YSZ interface. A model was proposed, following the reaction model of Verkerk [3,10], in which the rate was controlled by surface diffusion of oxygen atoms on the Pt electrode towards the three phase boundary. A schematic drawing of the reaction path is shown in fig. 9. At a distance $x=\delta$ from the Pt/YSZ interface, the oxygen activity at the Pt electrode was assumed to be in equilibrium with that in the gas phase. At the electrode a mean current density of the following form is obtained:

$$I_F = -\left[\frac{2FB\lambda\Gamma RT}{\delta}\right]\left[\frac{a_O^* P_{O_2}^{1/2}}{a_O^* + P_{O_2}^{1/2}}\right]\times \left[\frac{(1-\exp(2F\eta/RT))}{(a_O^* + P_{O_2}^{1/2}\exp(2F\eta/RT))}\right] \qquad (36)$$

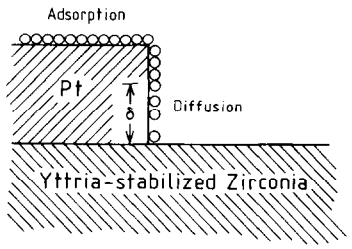

Fig.9 Schematic representation of mass transport of oxygen species, adsorbed on the metal electrode, towards the triple phase boundary according to the reaction models of [3] and [11].

where:

λ = constant proportional to the mobility of adsorbed oxygen atoms

Γ = surface concentration of oxygen adsorption sites

B = length of the three phase boundary in the unit area of the electrode

a_O^* = oxygen activity at which $\theta = 1/2$

The graphical representation of eq. (36) is shown in fig. 10. Limiting currents are predicted at relative low values of the overpotential. No Tafel behaviour can be explained with this model.

2.3.2. *Electrode impedance*

The analysis of the electrode impedance when mass

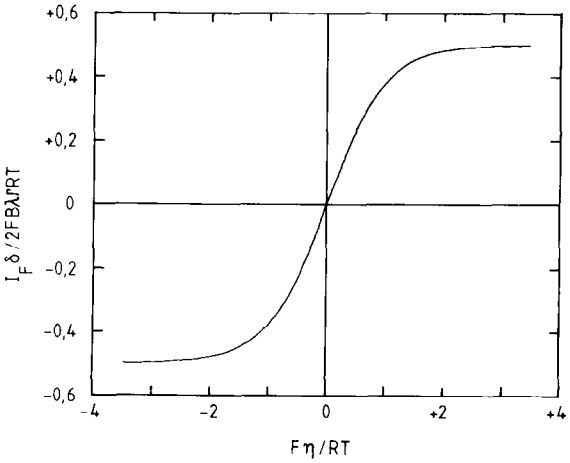

Fig.10 Simulated current-overpotential curve according to the reaction model of Mizusaki et al. [11], see eq. (36). Oxygen partial pressure was chosen as: $(PO_2/PO_2^*)=1$ where $PO_2^*=(a_O^*)^2$.

transport is rate determining was presented by Verkerk et al. [10], following the analysis of Broers [29]. This analysis is reformulated here in a somewhat different form. For the oxygen exchange reaction, the Butler-Volmer equation is used as shown in eq. (24). For small overpotentials, $\eta << F/RT$, eq. (24) can be lincarized and we obtain:

$$I_F = I_o \left(\frac{2F\eta}{RT} - \frac{(\theta-\theta_{eq})}{\theta_{eq}(1-\theta_{eq})} \right) \tag{37}$$

If the electrode potential is modulated in a sinusoidal manner with an excitation voltage $\Delta\eta\exp(j\omega t)$, this results in a modulation of the current, $\Delta I_F\exp(j\omega t)$ and the fraction of coverage of the adsorbed oxygen species, $\Delta\theta\exp(j\omega t)$. The amplitude of the current modulation is obtained from a first order Taylor expansion limited to first order terms of eq. (37), which results in:

$$\Delta I_F = I_o \left(\frac{2F\Delta\eta}{RT} - \frac{\Delta\theta}{\theta_{eq}(1-\theta_{eq})} \right) \tag{38}$$

The fraction of coverage of the adsorbed oxygen species is determined by the following mass balance equation:

$$\left(\frac{d\theta}{dt} \right) = D \left(\frac{d^2\theta}{dx^2} \right) \tag{39}$$

The modulation of the fraction of coverage of the adsorbed oxygen species is once again given by eq. (18). Substitution of eq. (18) in eq. (39) results after eliminating the $\exp(j\omega t)$ terms in:

$$j\omega \left(\frac{d\Delta\theta}{dt} \right) = D \left(\frac{d^2\Delta\theta}{dx^2} \right) \tag{40}$$

At a distance $x=\delta$ from the three phase boundary it is assumed that the fraction of coverage of the adsorbed oxygen species is constant:

$$\Delta\theta_{(x=\delta)} = 0 \tag{41}$$

With this boundary condition the solution of the second order differential eq. (40) is:

$$\Delta\theta(x) = -2M\exp\left(-\delta\sqrt{\frac{j\omega}{D}} \right) \sinh\left((x-\delta)\sqrt{\frac{j\omega}{D}} \right) \tag{42}$$

where M is an integration constant. $\Delta\theta(x)$ gives the amplitude of the modulation of the fraction of coverage of the adsorbed oxygen species in between the three phase boundary ($x=0$) and the electrode surface at $x=\delta$. Adsorption of oxygen is considered negligible in the area from $x=0$ to $x=\delta$. This means that the rate of diffusion is assumed to be fast in comparison with the rate of adsorption in this area. The current modulation at the electrode is given by:

$$\Delta I_F = -2FD\Gamma \left(\frac{d\Delta\theta}{dx} \right)_{x=0} \tag{43}$$

Combining eq. (42) and (43) gives:

$$\left(\frac{\Delta\theta}{\Delta I_F} \right) = \frac{1}{2FD\Gamma} \frac{\tanh\left(\delta\sqrt{\frac{j\omega}{D}} \right)}{\sqrt{\frac{j\omega}{D}}} \tag{44}$$

Substitution of eq. (44) in eq. (38) results in the following expression for the faradaic impedance of the electrode:

$$Z_F = \left(\frac{\Delta\eta}{\Delta I_F} \right) = R_{ct} + Z_W \tag{46}$$

where:

$$R_{ct} = \frac{RT}{2FI_o} \tag{46}$$

and

$$Z_W = \frac{RT}{4F^2D} \frac{1}{\Gamma\,\theta_{eq}(1-\theta_{eq})} \frac{\tanh\left(\delta\sqrt{\frac{j\omega}{D}} \right)}{\sqrt{\frac{j\omega}{D}}} \tag{47}$$

Following Mizusaki et al. [11,12], it is assumed that the equilibrium exchange current density is infinitely high, and R_{ct} tends to zero. Z_W is commonly called the finite-length Warburg impedance [30]. The graphical representation of eq. (47) is shown in fig. 11. When the penetration depth of the concentration perturbation ($\lambda=(2D/\omega)$) is small in comparison with the width of the diffusion layer (δ) then the Warburg impedance can be represented by a straight line making an angle of 45° with the real axis, and the diffusion occurs in an effectively semi-infinite medium. When the penetration depth is large in comparison with δ, than at high frequencies still the 45° straight line is observed but at low frequencies the Warburg impedance can be

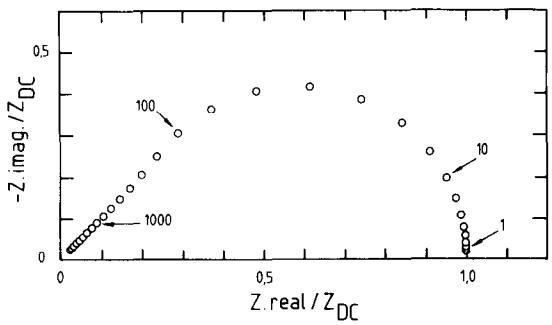

Fig.11 Warburg impedance following from the reaction model of Verkerk et al. [10] whith mass transport rate determining $(\delta^2/(2D))=5x10^{-3}$ sec). Frequencies indicated in Hz.

presented by a resistance in parallel with a pseudo capacitance. In this case the diffusion is limited by the width of the diffusion layer.

When the impedance diagrams of figs 4, 8 and 11 are compared to each other than it can be concluded that it is easy to distinguish this diffusional behaviour from the charge transfer processes discussed in the sections 2.2 and 2.3.

3. Conclusions

Original results are obtained for the electrode impedance when charge transfer at the Au,O_2(g)/yttria stabilized zirconia interface is rate determining. The most important result of this analysis is that when a stepwise electron transfer occurs to adsorbed intermediates inductive effects can be predicted in the impedance diagram. The inductive effects can be simulated at cathodic and anodic overpotentials. The inductive effect at cathodic overpotentials is related to an increase of the fraction of coverage of one of the adsorbed oxygen species when the cathodic overpotential becomes more negative.

When a competition exists between charge transfer and mass transport along the electrode/solid electrolyte interface, apparent Tafel behaviour can be observed. This model has been worked out for both associative and dissociative adsorption of oxygen. A rectangular electrode geometry was chosen for the mass transport problem. When the charge transfer process is described by a Bulter-Volmer equation with real charge transfer coefficients of $\alpha_c=\alpha_a=1$ this results in a current-overpotential curve with apparent charge transfer coefficients of $\alpha_c=0.5$ and $\alpha_a=1.5$. An important change occurs in the oxygen partial pressure dependence of the equilibrium exchange current density. For the charge transfer process the equilibrium exchange current density is proportional to the oxygen partial pressure as $I_o \propto PO_2^{1/4}$ which changes into $I_o \propto PO_2^{5/8}$ when a competition occurs with mass transport along the electrode/solid electrolyte interface. When a stepwise electron transfer occurs in the basic charge transfer mechanism inductive effects in the electrode impedance remain possible but no explicit results have been obtained. The only available treatment of the electrode impedance for a charge transfer process in competition with mass transport revealed a capacitive loop in the impedance diagram under equilibrium conditions.

When mass transport is rate determining limiting currents are predicted. Such a model does not result in inductive effects in the electrode impedance diagram but results in a Warburg diffusion element.

Acknowledgment

The investigations were supported by the Netherlands Foundation for Chemical Research (SON) with financial aid from the Netherlands Organisation for Scientific Research (NWO).

APPENDIX

A.1. General relations between reaction model parameters and real charge transfer coefficients.

The Butler-Volmer equation is expressed in the following form:

$$I_F = I_o(\exp(\alpha_a F\eta/RT) - \exp(-\alpha_c F\eta/RT)) \qquad (A1)$$

where:

I_o=equilibrium exchange current density
α_a=real anodic charge transfer coefficient
α_c=real cathodic charge transfer coefficient

This Butler-Volmer equation results from a particular charge transfer mechanism with the following parameters. The total number of electrons (n) transfered to molecular oxygen is n=4. The number of electrons transfered in the rate determining step is r. The number of times that the rate determining step takes place in order to transfer all n electrons to oxygen is ν. The total number of electrons that is transfered before or after the rate determining step is γ_b and γ_a, respectively. Making a local equilibrium approach for

all steps except the rate determining step, than the following relations hold [23]:

$$\alpha_a = \frac{\gamma_a}{\nu} + r(1-\beta) \tag{A2}$$

$$\alpha_c = \frac{\gamma_b}{\nu} + r\beta \tag{A3}$$

$$\alpha_a + \alpha_c = \frac{n}{\nu} \tag{A4}$$

where β is the symmetry coefficient of the rate determining step. If adsorbed intermediates are present than it is assumed that their fraction of coverage is small. The equilibrium exchange current density depends on the oxygen partial pressure as:

$$I_o \propto \left(P_{O_2}\right)^m \tag{A5}$$

As shown by Winnubst et al. [4], the oxygen partial pressure dependence of I_o depends on whether electrons are transfered in the rate determining step to atomic oxygen or molecular oxygen. Depending on those two possibilities the following relation holds between m and the real charge transfer coefficients:

$$m = \frac{\alpha_a}{2(\alpha_a + \alpha_c)} \qquad \text{(atomic oxygen)} \tag{A6}$$

$$m = \frac{\alpha_a}{(\alpha_a + \alpha_c)} \qquad \text{(molecular oxygen)} \tag{A7}$$

In eqs (A6) and (A7) it is assumed that the fraction of coverage of the adsorbed oxygen species is small.

A.2. Mathematical expressions for the equivalent circuit elements in the circuit of fig. 3.

When all partial derivatives are abbreviated as follows:

$$A = \frac{d}{d\Gamma\theta_1}\left(\frac{d\Gamma\theta_1}{dt}\right)_{E,\theta_2} \tag{A8}$$

$$B = \frac{d}{d\Gamma\theta_2}\left(\frac{d\Gamma\theta_1}{dt}\right)_{E,\theta_1} \tag{A9}$$

$$C = \frac{d}{dE}\left(\frac{d\Gamma\theta_1}{dt}\right)_{\theta_1,\theta_2} \tag{A10}$$

$$D = \frac{d}{d\Gamma\theta_1}\left(\frac{d\Gamma\theta_2}{dt}\right)_{E,\theta_2} \tag{A11}$$

$$E = \frac{d}{d\Gamma\theta_2}\left(\frac{d\Gamma\theta_2}{dt}\right)_{E,\theta_1} \tag{A12}$$

$$F = \frac{d}{dE}\left(\frac{d\Gamma\theta_2}{dt}\right)_{\theta_1,\theta_2} \tag{A13}$$

$$G = \left(\frac{dI_F}{d\Gamma\theta_1}\right)_{E,\theta_2} \tag{A14}$$

$$H = \left(\frac{dI_F}{d\Gamma\theta_2}\right)_{E,\theta_1} \tag{A15}$$

$$I = \left(\frac{dI_F}{dE}\right)_{\theta_1,\theta_2} \tag{A16}$$

than the following expression is obtained for the Faradaic impedance:

$$Z_F = \frac{1}{I} + \frac{-\left[\frac{G}{I}\right]\left[-\frac{CE}{I}+\frac{FB}{I}\right]-\left[\frac{H}{I}\right]\left[-\frac{AF}{I}+\frac{CD}{I}\right]-\left[\left[\frac{G}{I}\right]\left[\frac{C}{I}\right]+\left[\frac{H}{I}\right]\left[\frac{F}{I}\right]\right]j\omega}{\left[-E+\frac{FH}{I}\right]\left[-A+\frac{GC}{I}\right]-\left[D-\frac{FG}{I}\right]\left[B-\frac{CH}{I}\right]-\omega^2+j\omega\left[\left[-A+\frac{GC}{I}\right]+\left[-E+\frac{FH}{I}\right]\right]} \tag{A17}$$

The form of this expression is identical to the one for the equivalent circuit of fig. 3, with:

$$R_{ct} = \frac{1}{I} \tag{A18}$$

$$C_{ad} = \frac{-I^2}{(GC+HF)} \tag{A19}$$

$$\frac{1}{R_2} = C_{ad}\left[\left[-A+\frac{GC}{I}\right]+\left[-E+\frac{FH}{I}\right]\right]+(C_{ad})^2\left[\left[\frac{G}{I}\right]\left[-\frac{CE}{I}+\frac{FB}{I}\right]+\left[\frac{H}{I}\right]\left[-\frac{AF}{I}+\frac{CD}{I}\right]\right] \tag{A20}$$

$$\frac{1}{C_{ad}L_{ad}} = \left[\frac{\left[\frac{G}{I}\right]\left[-\frac{CE}{I}+\frac{FB}{I}\right]+\left[\frac{H}{I}\right]\left[-\frac{AF}{I}+\frac{CD}{I}\right]}{R_2}\right]+\left[\left[-E+\frac{FH}{I}\right]\left[-A+\frac{GC}{I}\right]-\left[D-\frac{FG}{I}\right]\left[B-\frac{CH}{I}\right]\right] \tag{A21}$$

$$R_1 = -C_{ad}L_{ad}\left[\left[\frac{G}{I}\right]\left[-\frac{CE}{I}+\frac{FB}{I}\right]+\left[\frac{H}{I}\right]\left[-\frac{AF}{I}+\frac{CD}{I}\right]\right] \tag{A22}$$

References

[1] E.C. Subbarao and H.S. Maiti, Solid State Ionics **11** (1984) 317.

[2] H. Okamoto, G. Kawamura, T. Kudo, Electrochimica Acta **28** (1983) 379.

[3] M.J. Verkerk, M.W.J. Hammink and A.J. Burggraaf, J. Electrochem. Soc. **130** (1983) 70.

[4] A.J.A. Winnubst, A.H.A. Scharenborg and A.J. Burggraaf, Solid State Ionics **14** (1984) 319.

[5] Da Yu Wang and A.S. Nowick, J. Electrochem. Soc. **128** (1981) 55.

[6] I.V. Murygin and V.N. Chebotin, Soviet Electrochem. Engl. Tr. **15** (1977) 1647.

[7] B.C. Nguyen, L.M. Rincon-Rubio and D.M. Mason, J. Electrochem. Soc. **133** (1986) 1860.

[8] N.L. Robertson and J.N. Michaels, AIChE (Symp. series 254) **83** (1987) 56.

[9] D.R. Franceschetti and A.P. Ross, Appl. Phys. **A49** (1989) 111.

[10] M.J. Verkerk, M.V.J. Hammink and A.J. Burggraaf, J. Electrochem. Soc. **130** (1983) 78.

[11] J. Mizusaki, K. Amano, S. Yamauchi and K. Fueki, Solid State Ionics **22** (1987) 313.

[12] J. Mizusaki, K. Amano, S. Yamauchi and K. Fueki, Solid State Ionics **22** (1987) 323.

[13] B.A. van Hassel, B.A. Boukamp and A.J. Burggraaf, *'Electrode Polarisation at the Au,O_2(g)/yttria stabilized zirconia interface. Part II: electrochemical measurements and analysis'*, Solid State Ionics, in press.

[14] M. Che and A.J. Tench, Advances in Catalysis, Vol. 31, 77.

[15] M. Che and A.J. Tench, Advances in Catalysis, Vol. 32, 1.

[16] M. Steinberg and A. Eyal, Appl. Surf. Sci. **8** (1981) 431.

[17] M. Setaka, S. Fukuzawa, Y. Kirino and T. Kwan, Chem. Pharm. Bull. **16** (1968) 1240.

[18] C. Li, K. Domen, K.-I. Maruya and T. Onishi, J. Cat. **123** (1990) 436.

[19] C. Gabrielli, Identification of electrochemical processes by frequency response analysis, Solartron Instrumentation Group, Farnborough, Technical Report Number 004/83 (1984).

[20] J.-P. Diard, B. Le Gorrec and C. Montella, J. Electroanal. Chem. **205** (1986) 77.

[21] J.-P. Diard, B. Le Gorrec and C. Montella, J. Electroanal. Chem. **255** (1988) 1.

[22] A.J. Bard and L.R. Faulkner, Electrochemical Methods, fundamentals and applications, John Wiley & Sons, New York, Chicheste, Brisbane, Toronto (1980).

[23] J. O'M. Bockris and A.K.N. Reddy, Modern Electrochemistry, Vol. 2, Plenum, New York, 1970.
[24] I.Epelboin, M.Ksouri and R.Wiart, J.Electroanal.Chem **65** (1975) 373.
[25] E.J.L. Schouler and M. Kleitz, J. Electrochem. Soc. **134** (1987) 1045.
[26] H.Yanagida, R.J.Brook and F.A.Kröger, J. Electrochem. Soc. **117** (1970) 593.
[27] B.A. van Hassel, Transport and oxygen transfer properties of ion implanted yttria stabilized zirconia, PhD Thesis, University of Twente, Enschede, The Netherlands (1990).
[28] D.R. Franceschetti and J.R. Macdonald, J. Electroanal. Chem. **101** (1979) 307.
[29] G.H.J. Broers and M. Schenke, Proc. Int. Conf. on Fuel Cells, Akademie Verlag, Dresden (1967), p. 299.
[30] H.T. Cahen, thesis, State University of Utrecht, 1980.